# Study of point-supported glass breakage behavior with varying point-covered areas under thermal loading

# Study of point-supported glass breakage behavior with varying point-covered areas under thermal loading

**Wei Lu[a], Haodong Chen[a], Yu Wang [b], Qiangling Duan[a], Lin Jiang[a], Qingsong Wang[a], Jinhua Sun [a,*]**

[a]*State Key Laboratory of Fire Science, University of Science and Technology of China, Hefei 230027, P.R. China*

[b]*School of Engineering, BRE Centre for Fire Safety Engineering, University of Edinburgh, Edinburgh EH9 3JL, United Kingdom*

**Abstract**

Point-supported glazing assemblies are widely used in modern buildings for aesthetic elegance, as well as for economic reasons. However, the formation of vents caused by glass breakage could aggravate ventilation controlled compartment fires. The point-covered area generally varies and may constitute potential fire hazards. Accordingly, it is necessary to investigate the fire performance and breakage mechanisms in various point-covered areas. In this study, a total of 12 tests, including three various point-covered area glazing, were heated by a 200 × 200 $mm^2$ pool fire. The breakage time, glass surface and air temperatures, incident heat flux, and crack initiation and final fall out ratio were obtained. The critical conditions for the three aforementioned various point-covered area glazing were determined. The reference breakage times, $t_r$, which were calculated by assigning a failure probability of 0.1 to the two-parameter Weibull distribution were 119, 140, and 166 s. It was established that a relatively small point-covered area glazing can survive longer; the smaller the point-covered area was, the larger the final fallout ratio of glazing assemblies will be. Numerical simulations were performed to investigate the stress distribution on the glass pane, with breakage times well predicted. Accordingly, these results have implications on the fire resistance design for point-supported glazing assemblies.

**Key words:** point-supported glazing; fire; point-covered area; first breakage time; stress field distribution.

## 1. Introduction

In recent years, with the rapid development of glass production technology, various types of functional glass have been developed, further increasing their applications in the building industry sector. Glass curtain walls have become essential parts of building functionalization and diversification [1]. Thus, instead of four-edge covered glass facades, point-supported glass curtain walls are increasingly being employed in high-rise building envelopes for their aesthetic and flexible characteristics [2][3]. Although glass is not a type of combustible material under a fire environment, as it is a relatively

* Corresponding authors: Tel.: +86 551 63606425; fax: +86 551 6360 1669.
E-mail: sunjh@ustc.edu.cn (J.H. Sun)

fragile material compared with concrete or steel, it may easily crack and even fall out when subjected to fire, which would unavoidably detrimentally influence building structure stability and integrity [4][5]. Newly formed vents, which would supply more oxygen from the outside fresh air, could increase the growth of ventilation controlled enclosure fire and have a crucial contribution to the interactive-external tridimensional fire development. The extensive employ of point-supported installation of glass façades would inevitably introduce with it, not only aesthetics, but also risks associated with fire. Accordingly, it is essential to explore its specific fire performance.

In the 1st International Symposium on Fire Safety Science, Emmons highlighted that "glass breakage is an important fire structure problem" [6]. Thereby, Keski-Rahkonen [7][8] established a classic physical model to analyze its fracture mechanism when subjected to uneven thermal loads. Through an analytical method, it was determined that the covered edges were the most prone to cracking. Skelly et al., Pagni et al., and, Shield et al. [9][10][11][12] performed a series of experiments to validate a previous theoretical model and concluded that the critical temperature difference among edge-covered glazing was approximately 90 °C. Manzello [13] and Klassen et al. [14][15] investigated the fire performance of large-scale glazing under a real fire. Chow et al. [16] conducted fire tests concerning the heat transfer and smoke movement in a model box on part of a glass system with two panels. Recently, Debuyser et al.[17] heated monolithic and laminated glazing with a special focus on the heat transfer and developed a 1D heat transfer model to determine the evolution of the temperature profile as a result of a given incident heat flux. BREAK1 [18] and EASY [19] were developed to predict the cracking time. Through previous studies, several consensuses have been reached, such as the following: although various types of glass, installation forms, and external heat sources have remarkable influence on the fire performance of glazing, the major cause of glass rupture is the excessive tensile stress caused by inhomogeneous temperature distributions resulting from the presence of shaded areas, including the location of heat source relative to the glazing.

Nevertheless, previous studies concerning the fire performance of point-supported glass façade, which are typically supported by four points and extensively used as external façades of core wall structured buildings or partition walls, as shown in Fig. 1, were limited. Recently, Wang et al. [2][20] conducted experiments and numerical simulations concerning the fire response of point-supported glazing. In relation to the investigation of the influence of various point-covered areas, a geometric factor was introduced as a function of covered width, as proposed by Pagni et al. and Joshi et al. [21][22], to investigate the edge-covered width effect. Tofilo et al. [23] conducted an investigation to theoretically determine the influence of various covered widths on thermal stress by establishing an approximate solution for a long strip of glass pane. Chen et al. [24] conducted experiments concerning different shaded widths, ranging from 10 to 50 mm under radiant heat. It was established that various shaded widths of glass panes have a vital influence on breakage behavior, whereas previous studies discussed above, solely concentrated on the framed edge-covered glass façades, which

were generally covered by a nontransparent frame or gasket. To the best of our knowledge, there is no open literature concerning the influence of varying point-covered areas on point-supported glazing assemblies. In engineering practice, the supporting point-covered area typically varies, which may introduce a potential fire hazard. Thus, it is insufficient with respect to practical guidance and national fire codes on the fire performance of various point-supported areas. In consideration of the increasing adoption of point-supported glazing with different point-covered areas in modern buildings, it is essential to investigate the thermal breakage behavior and underlying heat transfer mechanism, which could enhance our comprehension of the breakage process and criteria.

**Fig. 1.** Point-supported glass curtain wall, USTC campus, Hefei.

## 2. Experimental setup

As shown in Fig. 2(a), the test equipment primarily consisted of four sections: heat source, cabinet for glass installation, temperature and incident heat flux measurement system, and mass-loss balance system. The cabinet had a vent in front of the glass installation, which could support combustion in a compartment space. The edge-polished float glass pane was mounted on a frame with four screws. To investigate the influence of different supporting point-covered areas, three different sizes of screw nuts, as illustrated in Fig. 2(b), made of 304 stainless steel with a heat conductivity of 16.2 W/(m·K) at 373 K, and with the same inner diameter and thickness, were adopted. The inner diameter and thickness were 10 and 4 mm, respectively, and were not changed in the course of the experiments. The outer diameters were 15, 30, and 45 mm. In order to make the experiment comparable to a real fire environment, four 10-mm diameter circular holes were drilled in each corner at a distance of 35 mm from the edge of the glazing. The glazing was located 300 mm above the ground and 300 mm away from the n-heptane pool fire in a 200×200-mm$^2$ pan, which was determined by a pre-experiment. Twelve 600×600×6-mm$^3$ float glasses made of identical materials by the same local manufacturer were selected. As shown in Fig. 2(c), the glass surface temperatures were determined by 15 1-mm diameter K-type sheathed thermocouples

(TCi), which were attached to the glass panes with high-temperature adhesive. The thermocouples were numbered TC1–TC10 (attached to the fire side surface), TC12–TC16, and TC1–TC10 (attached to the ambient side surface). In addition, a sheathed thermocouple, numbered TC 11, was set 5 mm in front of the glass to measure the air temperature. It should be noted that TC01, 03, 05, 07, 12, and 14 were attached to the point-covered areas to measure temperature variations in the experiments. Because of the effect of hot air disturbance and radiation, the uncertainty of temperature measurement was evaluated at ±5%, which was considerably less than that in compartment fire experiments (uncertainty 10–30%) [13][25]. To elaborate on the location of crack initiation, A, B, C, and D represent the hole edge on the top left corner, top right corner, bottom left corner, and bottom right corner, respectively, as the locations where the cracks initiated. The heat release rate (HRR) of n-heptane pool fire was calculated based on the mass-loss rate recorded using a 404×360-mm$^2$ METTLER TOLEDO XA32001L model of an electric balance with an accuracy of 0.1 g. Furthermore, a GTT-25-50-WF/R model of a Gordon total heat flux gauge with a measurement range of 0–50 kW/m$^2$ was used to determine the total incident heat flux, including the full-band radiation and convective heat at the exposed side. The gauge was set 10 mm from the right side of the glass pane (viewed from a digital video camera) and mounted flush to the surface of the glass. By this means, the gauge would be located as close as possible to the measurement location. This method had been used extensively in measuring the incident heat flux on the glass pane. An n-heptane pool with a 99% purity and 1-kg mass was used to simulate the real fire scene and to ensure the consistency of all experimental fire sources. During the stable combustion stage, the heat release rate reached 100–200 kW. Furthermore, a video camera with a framing rate of 50 frame/sec was employed to record glass breakage and fire development.

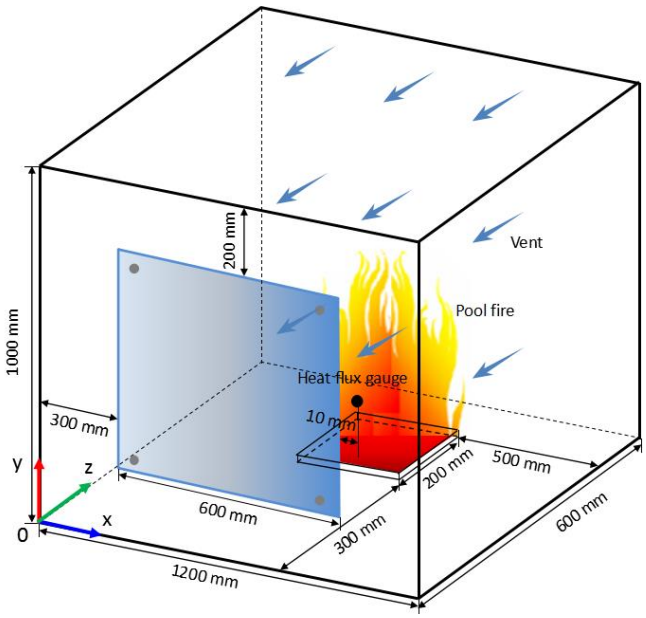


(a) Test apparatus.

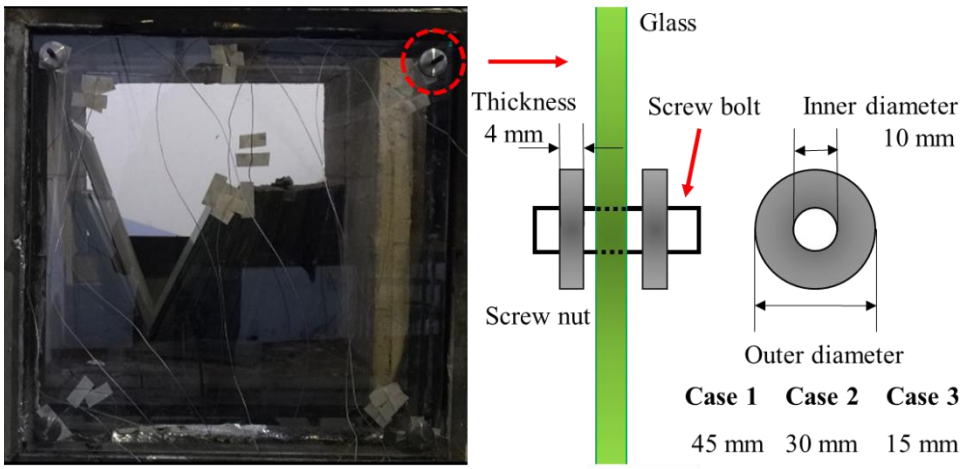


(b) Point-supported frame.

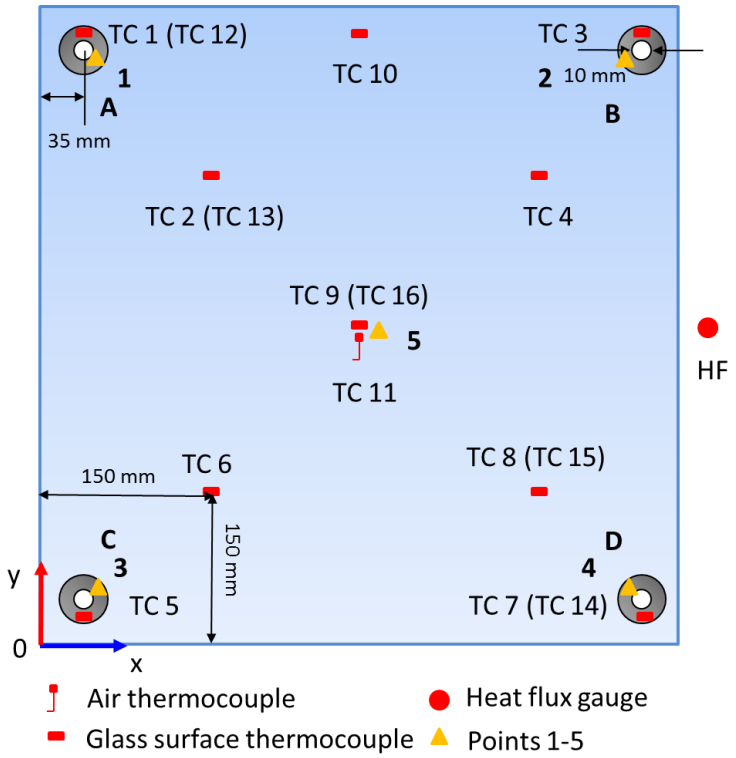


(c) The distribution of thermocouples and heat flux gauge

**Fig. 2.** The schematic of the experimental setup.

## . 3. Numerical methods

In a previous work [20], experiments were conducted to determine the stress on specific monitoring points on the glazing surface under fire-heated conditions. However, the measurement results were not able to show the overall stress distribution on the glass pane. Thus, for the purpose of revealing the stress distribution, an FEM software,

COMSOL Multiphysics, was employed to predict it. In this model, temperatures extracted from experimental data were loaded on the exposed side surface. It was supposed that the temperature variance at the ambient side was only caused by heat conduction from the exposed side surface. The dimensions and properties of the glass were identical with the glass pane used in the experiments, as summarized in Table 1. Grid independence tests were conducted to ensure the reliability and accuracy of simulation results. Consider Test 2 of Case 1 as an example. A total of 72 060 hexahedral elements, 19 972 quadrilateral elements, 1 472 edge elements, and 72 vertex elements were adopted based on the principle of time saving and accuracy, as shown in Fig. 3. The time interval was set to 1 s to guarantee the reliability and accuracy of results.

**Table 1**
Glass properties used in the simulation.

| Properties | Symbol | Value |
|---|---|---|
| Density (kg/m$^3$) | $\rho$ | 2500 |
| Modulus of elasticity (Pa) | $E$ | $7.2\times10^{10}$ |
| Poisson's ratio | $v$ | 0.20 |
| Thermal expansion coefficient (1/K) | $\beta$ | $8.75\times10^{-6}$ |
| Reference temperature (K) | $T_R$ | 293 |
| Specific heat capacity (J/(kg·K)) | $c_p$ | 703 |
| Thermal conductivity (W/(m·K)) | $k$ | 1.38 |
| Ultimate tensile strength (Pa) | $S_{ut}$ | $5\times10^{7}$ |
| Ultimate compressive strength (Pa) | $S_{uc}$ | $5\times10^{8}$ |

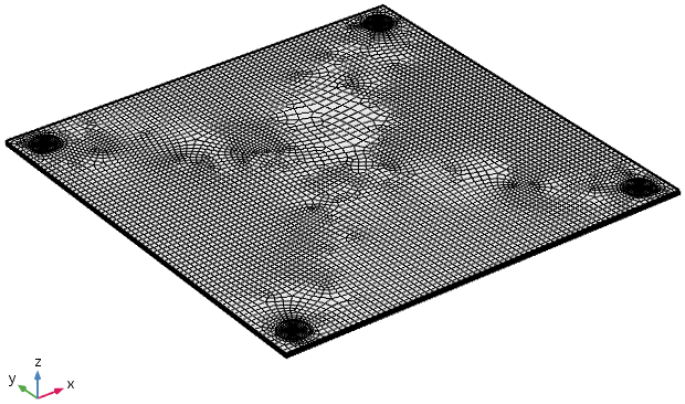


**Fig. 3.** Mesh grids in Test 1 of Case 3.

### 3.1. Heat transfer model

In this finite model, the temperature increase was mainly caused by the total incident heat flux, including the fire source radiation and air convection, which can be expressed by the heat transfer equation [22]:

$$\rho c \frac{\partial T}{\partial t} = k \frac{\partial^2 T}{\partial z^2} + Q \quad (1)$$

where, $\rho$, $c$, and $k$ are the density, specific heat, and thermal conductivity of the glazing, respectively, and $Q$ represents the total incident heat flux. The heat transfer progress of this finite model can be expressed by the total incident heat flux received by the exposed side of the glass pane. Furthermore, heat is radiated to the surroundings, convected with air, and conducted to the glass pane. Test 2 of Case 1, Test 2 of Case 2, and Test 1 of Case 3 were selected to predict the stress distribution and crack initiation. The experimental temperatures obtained by thermocouples were used in the simulation. Because of the limitation of thermocouples, which were arranged during the experiments according to the temperature distribution, a total of five regions were divided to load the temperature extracted from experiments, as shown in Fig. 2(c). For region 5, the average temperature measured by six thermocouples (TC 2, 4, 6, 8, 9, and 10) in this region was considered as the input temperature. For regions 1, 2, 3, and 4, the temperatures measured by TC1, 3, 5, and 07 were regarded as input temperatures, respectively.

### 3.2. Thermal stress model

The experimental results suggested that the glass pane was constrained in the $z$ direction at the edge of the support point. Consequently, it was assumed that the displacement in the $z$ direction was zero. To avoid rigid body displacement during the numerical simulation process, it was necessary to add simple constraints on two sides at the bottom of the glass pane. Generally, constraints cause stresses near the constrained boundaries when the structure undergoes temperature changes. Typically, thermal stress has a spatial distribution, as given by the following:

$$(\lambda + 2G)\nabla^2 e - \alpha \nabla^2 T = 0 \quad (2)$$

where, $\lambda$, $G$, and $e$ denote Lame coefficient, shear modulus of elasticity, and volumetric strain, respectively; $\alpha$ represents the thermal expansion coefficient. The quantities $\lambda$, $G$, and $e$ are expressed as follows:

$$\lambda = \frac{E\nu}{(1+\nu)(1-2\nu)},\ G = \frac{E}{2(1+\nu)},\ e = \varepsilon_x + \varepsilon_y + \varepsilon_z \quad (3)$$

where, $\nu$ is Poisson's ratio, and $\varepsilon_x$, $\varepsilon_y$, and $\varepsilon_z$ are the strains in the x, y, and z directions.

If the strain field satisfies the general compatibility relations, then, in principle, it is possible to integrate the above relationships. The procedure is outlined as follows [26]:

$$\varepsilon_{ij} = \frac{1}{2}\left(\frac{\partial u_i}{\partial X_j} + \frac{\partial u_j}{\partial x_i}\right) \quad (4)$$

$$u_i(\mathrm{X}) = u_i(\mathrm{X}_0) + \int_{\mathrm{X}_0}^{\mathrm{X}} \left(\varepsilon_{il} + (X_k - X_k^{'})\left(\frac{\partial \varepsilon_{il}}{\partial X_k} - \frac{\partial \varepsilon_{kl}}{\partial X_i}\right)\right) dX_l^{'} \quad (5)$$

The distance along the integration path can be parameterized by s, ranging from 0 to 1. This integral can be calculated as long as the strain field is an explicit function of the material frame coordinate, X.

$$X' = X_0 + s \quad (6)$$

$$u_i(X) = \int_0^1 (\varepsilon_{ij} + (1-s)p\,(\frac{\partial \varepsilon_{ij}}{\partial X_k} - \frac{\partial \varepsilon_{kj}}{\partial X_i}))\,p\,ds \quad (7)$$

### 3.3. Crack model

The crack initiation of the glass pane is random and uncertain. Generally, the larger the thermal stress is, the greater the possibility of cracking would be. In addition, glass has critical tensile and compressive strengths. Therefore, it is feasible to determine the glass crack initiation behavior by comparing the thermal stress with the critical tensile strength. Accordingly, the Coulomb–Mohr criterion was applied to determine crack initiation [19]. Crack occurs when the maximum and minimum principal stresses combine for a condition that satisfies the following equation:

$$\frac{S_1}{S_{ut}} - \frac{S_3}{S_{uc}} \geq 1 \quad (8)$$

where, $S_{ut}$ and $S_{uc}$ are the ultimate tensile and compressive strengths, respectively. Both $S_3$ and $S_{uc}$ remain in compression (negative).

## 4. Experimental results and discussion

### 4.1. Total incident heat flux

The total incident heat flux is a significant parameter for analyzing the glass breakage behavior. Table 2 summarizes the incident heat fluxes at the exposed side at the time of the first breakage. Because the heat flux gauge was located 10 mm off the glazing, the measured values may have been slightly smaller than that at the center of the glazing. Nevertheless, this method was widely utilized to obtain this parameter in a previous study [13]. The present experimental results suggested that the values were distributed in the range of 11.48–24.01 kW/m$^2$ among the different cases. The critical heat flux for glass breakage varied significantly when the area of the point-covered changed. It could be concluded that when subjected to the same incident heat flux, the smaller point-covered glazing had better fire resistance, and thus, required a relatively longer time to reach the critical heat flux. In addition, it should be noted that the average heat flux was similar between Cases 2 and 3, mainly because the breakage of these two forms occurred when the n-heptane pool fire grew under a relatively stable state.

**Table 2**
The incident heat fluxes at the first breakage time.

| Case no. | Test no. | Heat flux at the first breakage time (kW/m$^2$) | Average (kW/m$^2$) |
|---|---|---|---|
| 1 | 1 | 11.48 | 12.95 |
| | 2 | 12.79 | |
| | 3 | 13.46 | |
| | 4 | 14.07 | |
| 2 | 1 | 21.75 | 21.13 |
| | 2 | 23.26 | |

| | | | |
|---|---|---|---|
| | 3 | 19.34 | |
| | 4 | 20.15 | |
| 3 | 1 | 20.34 | 22.47 |
| | 2 | 24.01 | |
| | 3 | 24.89 | |
| | 4 | 20.63 | |

The increase in glass temperature was primarily attributed to the fire source radiation and convection on the exposed side, which can be expressed as follows [27]:

$$\rho cL\frac{dT(0,t)}{dt}=q_{conv}+q_{rad} \tag{9}$$

$$q_{conv}=h_0\left[T_{0\infty}(t)-T(0,t)\right] \tag{10}$$

where $\rho$, $c$, and $L$ are the density, specific heat capacity, and thickness of the glass pane, respectively; $q_{conv}$ and $q_{rad}$ represent the convection heat flux and radiation heat flux, respectively; $h_0$, $T_{0\infty}$, and $T(0, t)$ denote the convective heat transfer coefficient, ambient air temperature, and glazing temperature at the exposed (fire) side, respectively.

Assuming a constant radiation heat flux, $q_{rad}$, and convective heat transfer coefficient, $h_0$, the glazing temperature rise may follow an exponential growth according to the following equation calculated by solving the above differential equations:

$$T(0,t)=\frac{q_{rad}}{h_0}\left(1-e^{-\frac{h_0}{\rho Lc}t}\right)+T_{0\infty} \tag{11}$$

where $T_{0\infty}$ is the initial glass pane temperature.

In this heat transfer model, the convection heat flux can be calculated from the ambient air temperature at the center of the exposed side. Because of the action of high temperature gas, the convective heat transfer coefficient of the exposed side, $h_0$, would vary during the experiments. In this study, we adopted the equation proposed by Pagni and Emmons, expressed as follows [28]:

$$h_0(t)=5+45\left[T_{0\infty}(t)-T(0,t)\right]/100 \tag{12}$$

Note that when $h_0$ is equal to 50 W/(m·K), this value will be retained and remain unchanged.

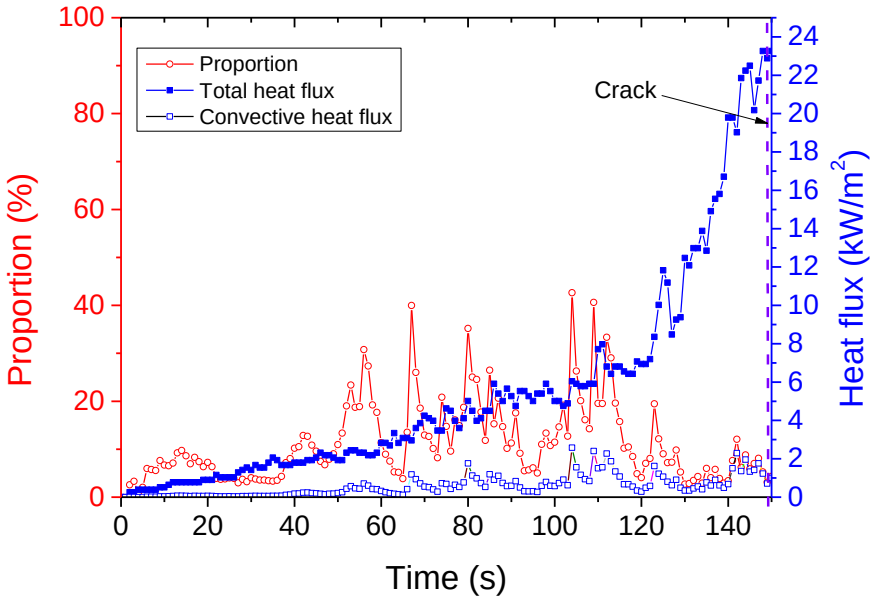


**Fig. 4.** Proportion of convective heat flux.

Consider Test 2 of Case 2 as an example. Figure 4 illustrates the variance of the incident heat flux on the glass panes. It was found that the first breakage occurred at 135 s, and the total incident heat flux fluctuated in the range 0–23 kW/m$^2$ before the occurrence of this first breakage. The air temperature at the exposed (fire) side was higher than the temperature of the glass surface and rapidly rose after ignition. In the figure, the proportion of the heat convection is represented with a red curve. The results suggested that before 50 s, the glazing temperature gradually rose, whereas the air temperature rapidly increased because of the direct heat radiation and convection from the fire source, which resulted in the corresponding rapid increase in the proportion of heat convection. Thereby, under the combined action of the fire source radiation and heat convection, the temperature of the glazing rapidly increased. However, because a considerable amount of hot gas accumulated in the confined space, it was apparent that convective heat transfer had a significant influence on the temperature increase of the glass pane. This phenomenon further confirmed that convective heat transfer had a more significant function under such a condition than that in an open space fire because hot gas in open space would rapidly release heat to the external space. In a previous experiment [27] conducted with an open space fire, the convective heat transfer had no contribution to the temperature rise of the glass pane after 90 s because the gas temperature was lower than the glazing at the surface of the exposed side.

### 4.2. Heat release rate

The heat release rate is also a significant parameter for analyzing glass breakage. The change in the fuel mass was measured during the experiments, and HRR $\dot{Q}$ of the heat source in the 200×200 mm$^2$ square fuel pan was calculated using the following:

$$\dot{Q} = \alpha \times \dot{m} \times \Delta H \quad (13)$$

where, α is the combustion efficiency factor taken as 0.75 [29]; $\dot{m}$ is the mass-loss rate

of n-heptane, in kg/s; $\Delta H$ is the fuel combustion heat of n-heptane at 48 066 kJ/kg. The mass of n-heptane was approximately 1000 g, which could maintain combustion for more than 6 min. Consider Test 3 of Case 3 as an example, as shown in Fig. 5. It should be noted that the blue broken line, obtained by data fitting experimental results, would be a better representation of the heat release rate. The results suggested that the heat release rapidly rose after ignition, reached a relatively steady state, and finally, decreased. Thus, the whole combustion process could be divided into three stages: the rapid growth stage, relatively steady stage (75–145 kW), and decay stage. After ignition, the heat release rate reached a relatively steady stage within 37 s and remained at that stage for about 250 s, attaining a maximum value of 145 kW at 190 s. The first breakage occurred at 204 s, which was under a relatively stable combustion stage with a heat release rate of 121 kW. Based on 12 experimental results, it was concluded that the first breakage usually occurred when the combustion was in a relatively steady stage.

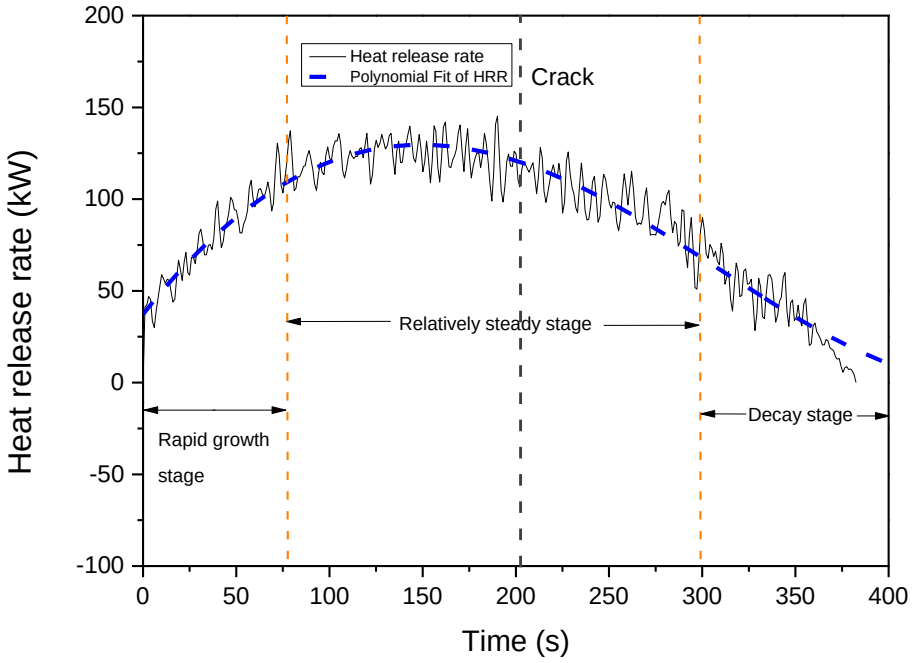


**Fig. 5.** Heat release rate in Test 3 of Case 3.

### 4.3. Time to the first breakage and fall out

The first breakage time is a particularly critical parameter for the analysis of glass breakage and fall out. After the glass pane cracked for the first time, “islands” were swiftly formed and the pane was considerably prone to fall out. On the one hand, glass fall out could result to the loss of glazing integrity, which would have a detrimental influence on the stability of the building structure. On the other hand, newly formed vents caused by glass breakage could provide a route for the entry of outside fresh air into the interior space and fuel the growth of ventilation-controlled enclosure fire. Accordingly, such vents have a crucial function in the development of an interactive-external tridimensional fire. As listed in Table 3, the first glass breakage times in four repeated experiments of the same case were similar. However, there was a significant

distinction among various point-covered areas, which indicated that such areas had an instantaneous influence on breakage times. It was found that the larger the point-covered area was, the shorter the breakage time will be. Thus, it can be concluded that a relatively smaller point-covered area has better fire resistance.

**Table 3**
The time to the first breakage.

| Case no. | The first breakage time (s) | | | | |
|---|---|---|---|---|---|
| | Test-1 | Test-2 | Test-3 | Test-4 | Average |
| 1 | 122 | 130 | 127 | 135 | 129 |
| 2 | 159 | 150 | 165 | 146 | 155 |
| 3 | 185 | 173 | 204 | 196 | 190 |

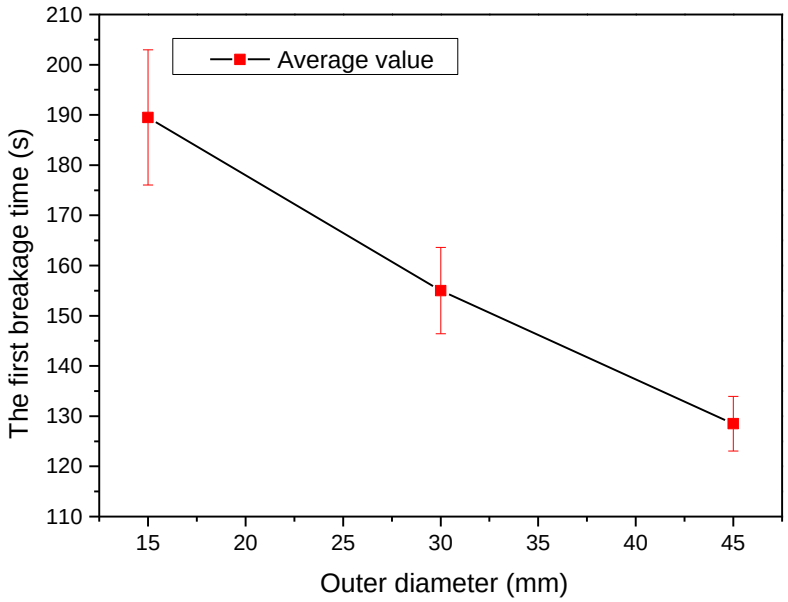


**Fig. 6.** The first breakage time.

Because initial minor imperfections or defects distributed along the edges of glazing and drilled holes are generally unavoidable because of the drilling process during fabrication [30], the edges were polished before the experiments were conducted to minimize the impact of these imperfections and defects on glass breakage to the extent possible. Despite all these, the breakage and fall out of glazing during fires remain stochastic [31]. Compared with theoretical and numerical studies, the repetition of experiments conducted under the same conditions for each case is a relatively accurate method to investigate the glass breakage phenomenon. In addition, the quantification of these impacts were performed using Weibull distribution functions by fitting the experimental data [11]. It is assumed that the first breakage time, t, satisfies this distribution, as follows [32]:

$$\varphi(t) = \left( \frac{t - t_u}{t_0} \right)^m \tag{14}$$

where, $t_u$ and $t_0$ denote the failure-free period and characteristic life, respectively, and $m$ is the shape factor. Thus, the foregoing described the lifetime distribution of the material. The Weibull ++ 7.0 software, based on the linear least squares fitting method, was employed to determine the characteristic life, $t_0$, and shape factor, $m$, of the Weibull distribution, as listed in Table 4. Furthermore, the failure probability function, F(t), is given by the following expression:

$$\mathrm{F}(t) = 1 - \exp\left[ -\left( \frac{t - t_u}{t_0} \right)^m \right] \tag{15}$$

The probability density function, f(t), which is the derivative of F(t), can be expressed as follows:

$$\mathrm{f}(t) = \frac{m}{t_0}\left( \frac{t - t_u}{t_0} \right)^{m-1} \exp\left[ -\left( \frac{t - t_u}{t_0} \right)^m \right] \tag{16}$$

**Table 4**

Parameters for the two-parameter Weibull distribution function of the first breakage time.

| Case no. | m | $t_0$ (s) | $t_u$ (s) | $t_r$ (s) |
|---|---|---|---|---|
| 1 | 23.61 | 131.05 | 0 | 119 |
| 2 | 17.69 | 159.07 | 0 | 140 |
| 3 | 14.02 | 195.71 | 0 | 166 |

The calculated values of $t_u$, $t_0$, and $m$ were substituted in Eqs. (15) and (16) to obtain the failure probability and probability density functions plotted in Fig. 7. It was found that the failure probability sharply increased at a certain point when the breakage times were more than approximately125, 150, and 175 s for Cases 1–3, respectively. It was noteworthy that the failure probability rose from approximately 0.1 to 1 with the smallest range 117–127 s for Case 1. The reference breakage times, $t_r$, which were calculated by setting the failure probability to 0.1, were essential to the fire-resistance design of glazing assemblies. For Cases 1–3, the breakage times, $t_r$, were 119, 140, and 166 s, respectively. The results further confirmed that glazing with relatively smaller point-covered areas had better fire-resistance when subjected to the same fire environment. The probability density function is plotted in Fig. 7(b). In addition, in a previous study pertaining to the influence of the edge-covered width for framing edge-covered glazing on fire performance [22], it was found that the first breakage times decreased as the edge-covered width increased. Thus, from the perspective of breakage time, a relatively smaller point-covered area and edge-covered width are recommended for point-supported and edge-covered glass curtain walls, respectively, under the premise of structural strength in engineering practice.

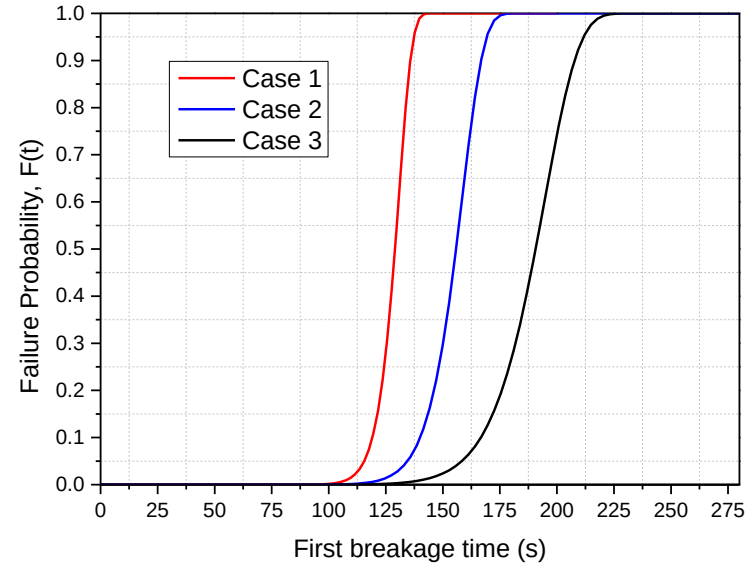


(a) Variation of the Weibull failure probability with the first breakage time.

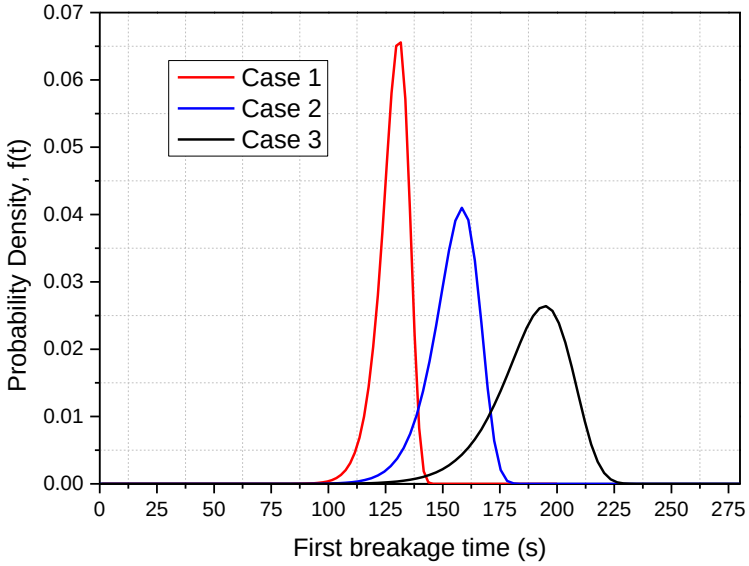


(b) Variation of the Weibull probability density function with the first breakage time.

**Fig. 7.** Weibull distribution results of the first breakage time.

It was found from experimental results that all cracks were initiated from the supported points; remarkably different from edge-covered framed glazing whose cracks consistently started from the edges of the glass pane [8]. The locations of the crack initiations and fall out ratios are summarized in Table 5. The crack initiation locations A, B, C, and D represent the hole edge at the top left corner, top right corner, bottom left corner, and bottom right corner, respectively. The locations of crack initiations were as follows: two tests at A, two tests at B, three tests at C, and eight tests at D. The excessive thermal stress caused by the temperature difference between the exposed and covered areas was the main reason for glazing cracking. Thus, the phenomenon may be attributed to a relatively high temperature difference at the bottom right corner (D). It is noteworthy that not all cracks initiated from a single supported point. The crack

initiation locations under Test 1 of Case 2, Test 2 of Case 2, and Test 4 of Case 3 were at (A, C, D) , (C, D) and (C, D), respectively. Figure 8 shows the fall out area ratio of glass panes over time. It was found that there were significant differences in the process of glass fall out among the three cases. It should be noted that the final fall out ratio of four repeated experiments in Case 1, with the maximum point-covered area, were all 0%, which indicated that fall out had the least possibility of occurring under this condition. Test 4 of Case 3 had the largest final fall out ratio at 11.2%, along with two main fracture processes. It was found that as the times of the main fracture process increased, the number of cracks would increase, forming more crack 'islands' because of crisscrossed cracks. Consequently, the probability of a fall out was increased. The primary reason for the fall out of the glazing when subjected to a confined space fire was the reduction in the constraint among the crack 'islands' and the impact of external disturbances, such as ambient wind load and flame entrainment. Nevertheless, the influence of the impact of external disturbances could be ignored because the cases had the same boundary conditions, except for different point-covered areas. Therefore, the various final fall out ratios were attributed to the decrease in constraints among the crack 'islands'. In the experiments, all crack initiations occurred at the supporting point edge After the cracks were initiated, they rapidly propagated and soon formed crack 'islands' near the supporting point edge and other locations because of crisscrossed cracks. If the crack 'islands' near the supporting point edge led to a fall out, then, the other crack 'islands' supported by the reactive forces provided by the former 'islands' would cause the glass pane to become considerably prone to a fall out [33]. Thus, a relatively large point-covered area would provide more restraint near the supporting point edge, which would further reduce the possibility of a fall out.

**Table 5**
The first breakage position and final fallout ratio.

| Case no. | Test no. | First breakage position | Final fallout ratio (%) |
|---|---|---|---|
| 1 | 1 | A | 0 |
| | 2 | D | 0 |
| | 3 | D | 0 |
| | 4 | D | 0 |
| 2 | 1 | A, C, D | 1.4 |
| | 2 | C, D | 2.1 |
| | 3 | D | 0 |
| | 4 | B | 0 |
| 3 | 1 | C | 5.4 |
| | 2 | D | 0.4 |
| | 3 | B | 9.7 |
| | 4 | C, D | 11.2 |

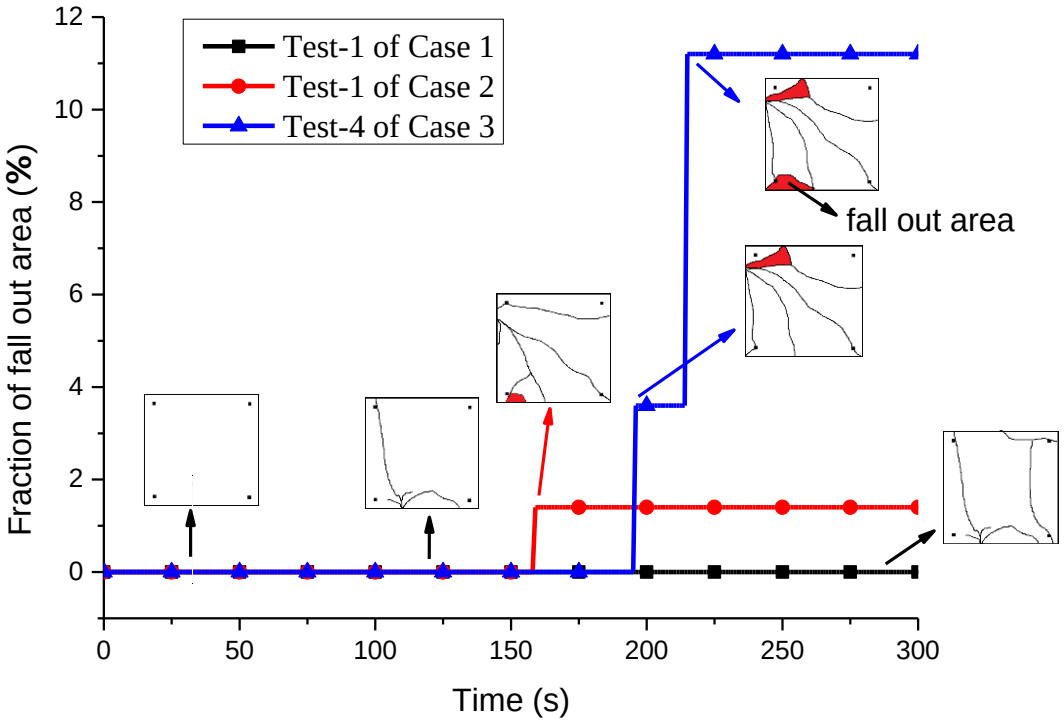


**Fig. 8.** Time histories of glass fall out.

### 4.4 Glass surface and ambient air temperatures

Sixteen K-type sheathed thermocouples were utilized to measure the temperatures of the ambient air and glass pane surface both on the exposed and ambient sides. This method had been used extensively to investigate the temperature distribution in glazing [2]. Consider Test 2 of Case 2 as an example. The temperature variation in the experiment is shown in Fig. 9(b). The first breakage occurred at 150 s and ambient air temperature at the exposed side was measured by TC11. After ignition, the ambient air temperature rapidly rose, and it was observed that the heating rate was higher than that at the glazing surface. It was found that the ambient air temperature was consistently at its highest because of the smoke aggregation in the confined space. Thus, the influence of thermal convection on the increase of glazing temperature was considerably significant than that in open space fire. Furthermore, the width of the fire plume was slightly smaller than that of the glazing, which resulted to a relatively substantial thermal gradient along the horizontal direction. Therefore, the temperatures measured by TC09 and 10, both located at the middle line of the glazing surface at the exposed side, were higher than those of other monitoring points. In addition, because of the hot gas that accumulated on the upper part of the cabinet under the action of buoyancy, the heat convection intensity at the upper part of the glass pane was relatively larger than that at the lower part. Consequently, the temperature measured by TC10 was higher than that measured by TC09. Although the center of the ambient side surface temperature (TC16) was relatively lower after ignition, because glass is a poor heat conductor, after 40 s, the temperature rapidly rose to a level considerably higher than those of other monitoring points at the ambient side. From an overall perspective, the

temperature measured at the exposed side surface was relatively higher than that at the ambient side surface, mainly because the radiant heat from the fire source was blocked by the glass frame. Thus, the ambient side surface was primarily heated through heat conduction from the exposed side surface. As for the comparison among the experimental results of the various cases that were conducted under the same fire condition, it was found that the most evident difference among them was the temperature variance of covered areas at the exposed and ambient side because of the different point-covered areas. The exposed area of the glass pane at the fire side was directly heated by the radiation and convection from the flames and hot gas, respectively. Thus, the rate of temperature increase at the exposed area was faster than that at the covered area. With the increased temperature at the point-covered area, the heating rate at that area significantly decreased. Therefore, breakage conditions are determined by the temperature difference between the exposed and point-covered areas. The temperature difference on the glazing surface is defined as follows:

$$T_h = \frac{T_2 + T_4 + T_6 + T_8 + T_9 + T_{10}}{6} \tag{17}$$

$$T_c = \frac{T_1 + T_3 + T_5 + T_7}{4} \tag{18}$$

$$\Delta T_{h-c} = T_h - T_c \tag{19}$$

where, $T_i$ is the temperature measured by TCi; $T_h$ is the average temperature of the exposed area on the exposed side; $T_c$ is the average temperature of the supporting point-covered area on the exposed side; $\Delta T_{h\text{-}c}$ is the temperature difference between these two regions. All critical values at the time of the first breakage are summarized in Table 6. It was found that for Case 1, temperature differences at breakage time were distributed in the range 117–126 °C, which is considerably lower than the range 122–142 °C calculated in Case 2 and 139–150 °C calculated in Case 3. These results further suggested that a relatively lager point-covered area had better fire resistance.

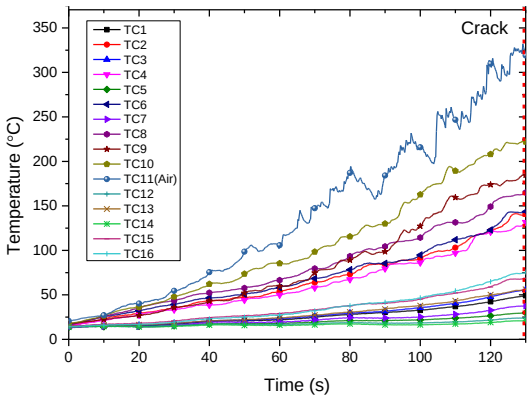


(a) Temperature variance in Test 2 of Case 1

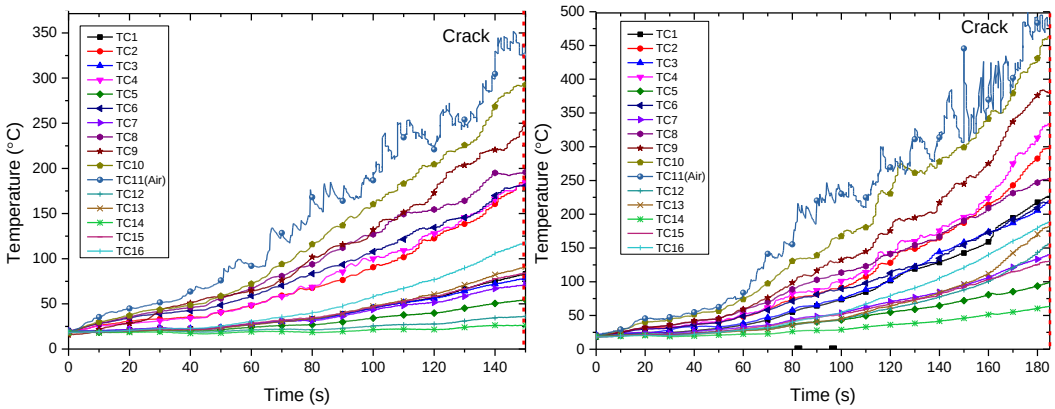


(b) Temperature variance in Test 2 of Case 2 (c) Temperature variance in Test 1 of Case 3

**Fig. 9.** Temperatures at different monitoring points.

**Table 6**

The temperatures at the time of the first breakage.

| Case no. | Test no. | Exposed center, $T_9$ (°C) | Ambient center, $T_{16}$ (°C) | Gas temperature, $T_{11}$ (°C) | Temperature difference, $\Delta T_{h-c}$ (°C) | Average (°C) |
|---|---|---|---|---|---|---|
| 1 | 1 | 222 | 105 | 388 | 117 | 122 |
| | 2 | 185 | 76 | 319 | 122 | |
| | 3 | 207 | 94 | 311 | 126 | |
| | 4 | 198 | 102 | 314 | 121 | |
| 2 | 1 | 245 | 127 | 327 | 133 | 134 |
| | 2 | 250 | 118 | 322 | 142 | |
| | 3 | 267 | 120 | 328 | 137 | |
| | 4 | 242 | 114 | 339 | 122 | |
| 3 | 1 | 378 | 190 | 485 | 150 | 146 |
| | 2 | 348 | 145 | 453 | 141 | |
| | 3 | 376 | 182 | 494 | 154 | |
| | 4 | 364 | 177 | 464 | 139 | |

## 5. Numerical results and comparison with experimental results

As summarized in Table 7, the maxima of the first principal stresses before the time of the first breakage were all around 50 MPa. These results suggested that the ultimate tensile strength was an essential parameter for predicting glass breakage. The first breakage times predicted by the simulation of Test 2 of Case 1, Test 2 of Case 2, and Test 1 of Case 3 were 131, 155, and 200 s, respectively, which agreed well with experimental results (130, 150, and 185 s, respectively). These results are within the allowable range because of the simplification of the boundary condition. It was found that $\sigma_{xx}$ was not consistent with $\sigma_{yy}$ primarily because of the asymmetry of the temperature field. The simulation results further suggested that the larger the point-covered area is, the shorter the first breakage time will be. Hence, the results of this numerical simulation have implications on the design for point-covered areas of point-

supported glass assemblies under the premise of structural strength.

**Table 7**
Numerical simulation results.

| Case no. | Test no. | First breakage time (s) | | $S_{1max}$ (MPa) | $\sigma_{xxmax}$ (MPa) | $\sigma_{yymax}$ (MPa) |
|---|---|---|---|---|---|---|
| | | Experiment | Simulation | | | |
| 1 | 2 | 130 | 131 | 50.97 | 44.19 | 44.33 |
| 2 | 2 | 150 | 155 | 50.66 | 49.11 | 47.72 |
| 3 | 1 | 185 | 200 | 50.91 | 48.94 | 48.79 |

To determine the location of crack initiation, the distributions of the first principal stresses in the *x* and *y* directions were calculated. Note that a stress greater than zero, represented tensile stress; otherwise, it represented compressive stress. Consider Test 2 of Case 1 as an example. Before the first breakage, the maximum stress, which was significantly larger than the stress in other regions, was located at the supporting point edge, as shown in Fig. 10(a). Moreover, the location of crack initiation, which satisfied the Coulomb–Mohr criterion, was also the location of the maximum of the first principal stress. The location of the crack initiation was consistent with the stress distribution. The results of other cases were similar to the above, where all cracks were initiated at the supporting point edge. It was observed from Fig. 10(b) that the maximum of the first principal stress appeared at the lower right, at the supporting point edge, which was subjected to the maximum tensile stress. It is noteworthy that the supporting point edge often had a large number of minor flaws or defects because of the drilling process, which made this area more prone to cracking. Furthermore, the glass pane was subjected to compressive stresses with a maximum of −25.27 MPa. However, glass compressive strength is 10 times a strong as tension. Therefore, it was easier to initiate cracks from these locations with the maximum tensile stress, which agreed well with experimental results.

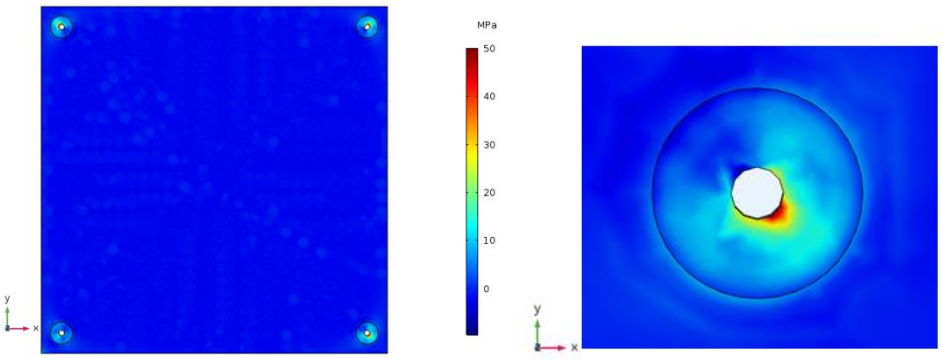


(a) First principal stress (b) First principal stress at the lower right of support point

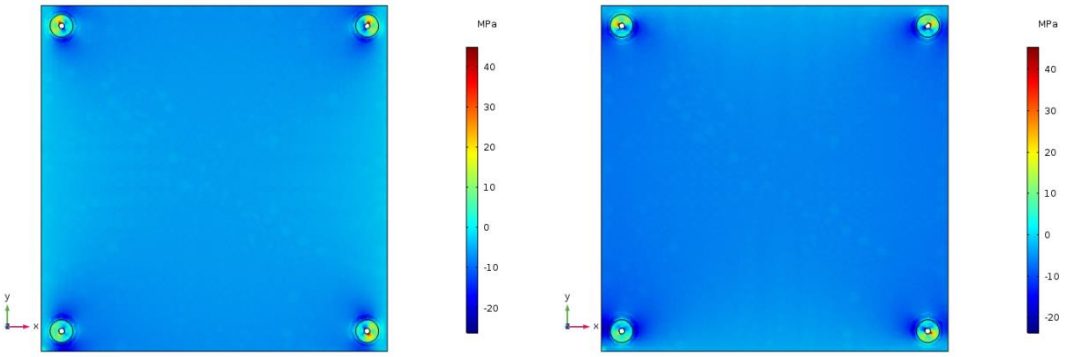


(c) Stress in the *x* direction (d) Stress in the *y* direction

**Fig. 10.** Stress distribution before the time of the first breakage (Test 2 of Case 1).

In order to provide a more intuitive understanding of the distribution of the first principal stress in the experiments, the first principal stress variance is illustrated in Fig. 11. Consider Fig. 11(e) as an example. Point 1 is located at the center of the glass pane and Points 2–5 represent the maximum values of the first principal stress in the point-covered regions. Because the central area had the same instantaneous temperature, the first principal stress at Point 1 was significantly smaller than those in other regions. As shown in Fig. 11(f), it was found that because of the increased temperature difference between the point-covered and exposed areas, the maximum stresses in the *x* and *y* directions, and the maximum principal stress, gradually increased. At the time of the first breakage, the maximum stresses in the *x* and *y* directions were 48.94 and 48.79MPa, respectively. The maximum stress in the *x* direction was not consistent with the *y* direction stress because of the asymmetry of the temperature field. The simulation results suggested that the trend of the first principal stress variance at Points 2–5 were practically similar to the stress trend shown in Fig. 11(f).

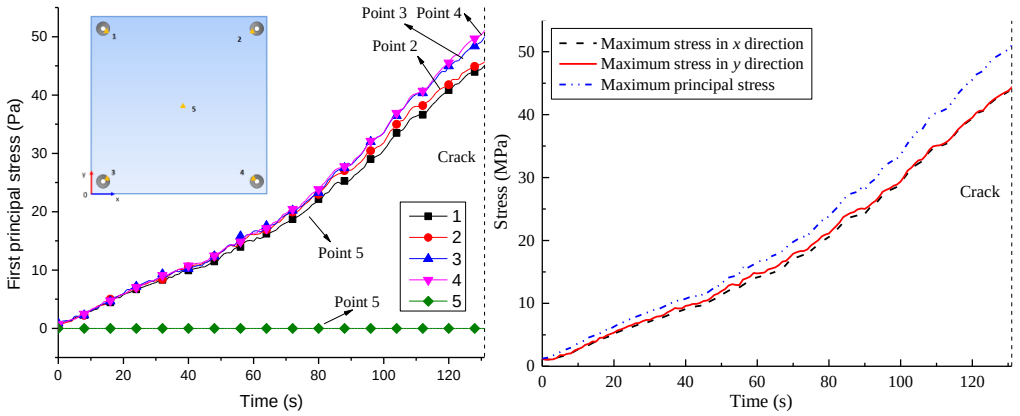


(a) First principal stress (b) maximum stress in the *x* and *y* directions, and maximum principal stress

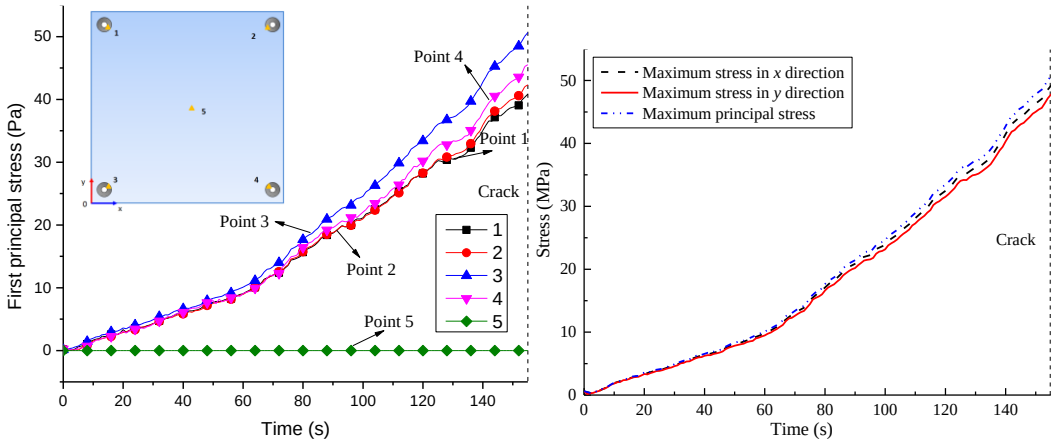


(c) First principal stress (d) maximum stress in the *x* and *y* directions, and maximum principal stress

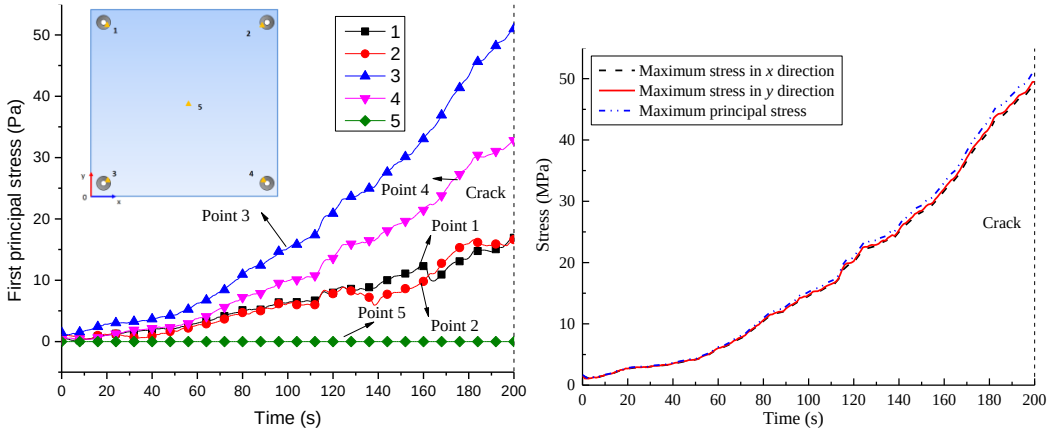


(e) First principal stress (f) maximum stress in the *x* and *y* directions, and maximum principal stress

**Fig. 11.** Stress variance in the simulation.

## 6. Conclusions

To determine the influence of various point-covered areas in a fire environment, 12 experiments were performed. A number of essential parameters, such as the first breakage time, final fall out ratio, incident heat flux, glass surface and ambient air temperatures, and heat release rate, were recorded to analyze the breakage behavior of the glazing assembly. Numerical simulation was employed to reveal the stress distribution, and predict the breakage time and crack initiation. The specific conclusions are as follows:

1. The experimental results suggested that the larger the supporting point-covered area was, the shorter the elapsed time was for the first cracking of the glazing assembly to occur. The reference breakage times, $t_r$, which were calculated by setting the failure probability to 0.1 of the two-parameter Weibull distribution, were 119, 140, and 166 s for Cases 1–3, respectively. Thus, from the perspective of breakage time, a relatively small point-covered area is recommended for the point-supported glass curtain walls under the premise of structural strength in engineering practice.

2. It was established that with the increase in the main fracture process times, the numbers of cracks would increase, and that the smaller the point-covered area is, the larger the final fall out ratio of glazing assemblies will be.
3. In this study, the first breakage time predicted by FEM analysis in relation to the effect of the drilled circular hole and point-covered area, agreed well with experimental results. Thus, the numerical model could be used in the fire-resistance evaluation of point-supported glazing assemblies.

**Acknowledgment**

This work is supported by the National Natural Science Foundation of China (Grant No. 51578524), the Fundamental Research Funds for the Central Universities (Grant No. WK2320000038), and the China Postdoctoral Science Foundation Project (Project No. 2017M612093). The authors sincerely thank the Editor U. Gross and three anonymous reviewers for their constructive reviews that have significantly improved the paper. The authors also thank Yijun Liu and Zhaoyu Wang for their help during the experiment.

Declaration of conflicting interests

The author(s) declared no potential conflicts of interest with respect to the research, authorship, and/or publication of this article.

**References**

[1] W. Chow, Building fire safety in the Far East, Archit Sci Rev, 48 (2005) 285-294.
[2] Y. Wang, Q.S. Wang, J.H. Sun, L.H. He, K.M. Liew, Effects of fixing point positions on thermal response of four point-supported glass facades, Constr. Build. Mater. , 73(2014) 235-246.
[3] C. Bedon, X. Zhang, F. Santos, D. Honfi, M. Kozłowski, M. Arrigoni, L. Figuli, D. Lange, Performance of structural glass facades under extreme loads-Design methods, existing research, current issues and trends, Construct. Build. Mater. 163 (2018) 921-937.
[4] L.H. Lin, E. Hinman, H.F. Stone, A.M. Roberts, Survey of window retrofit solutions for blast mitigation, J. Perform. Constr. Facil. 18 (2) (2004) 86-94.
[5] M. Wu, W. Chow, A review on fire-resistant glass with high rating, J. Appl. Fire Sci. 23 (1) (2013) 59-76.
[6] H. Emmons, The needed fire science, in: Fire Safety Science-Proceedings of the First International Symposium, IAFSS, Berkeley, California, 1986, 33-53.
[7] O. Keski-Rahkonen, Breaking of window glass close to fire, II: circular panes, Fire Mater., 15 (1991) 11-16.
[8] O. Keski-Rahkonen, Breaking of window glass close to fire, Fire Mater., 12 (1988) 61-69.
[9] J. Shields, G.W. Silcock, F. Flood, Behavior of double glazing in corner fires, Fire Technol., 41 (2005) 37-65.
[10] T.J. Shields, G.W.H. Silcock, M.F. Flood, Performance of a single glazing assembly exposed to enclosure corner fires of increasing severity, Fire Mater., 25 (2001) 123-152.
[11] A. A. Joshi, P.J. Pagni, Fire-induced thermal fields in window glass. II—

609 experiments, Fire Saf. J., 22 (1994) 45-65.
610 [12] M. J. Skelly, R.J. Roby, C.L. Beyler, An experimental investigation of glass
611 breakage in compartment fires, J. Fire. Prot. Eng., 3 (1991) 25-34.
612 [13] S.L. Manzello, R.G. Gann, S.R. Kukuck, K.R. Prasad, W.W. Jones, An
613 experimental determination of a real fire performance of a non-load bearing glass
614 wall assembly, Fire Technol., 43 (2007) 77-89.
615 [14] M.S. Klassen, J.A. Sutula, M.M. Holton, R.J. Roby, T. Izbicki, Transmission
616 through and breakage of multi-pane glazing due to radiant exposure, Fire Technol.,
617 42 (2006) 79-107.
618 [15] M.S. Klassen, J.A. Sutula, M.M. Holton, R.J. Transmission through and breakage
619 of single and multi-pane glazing due to radiant exposure: state of research. Fire
620 Technol., 46 (2010) 821-832.
621 [16] W.K. Chow, Y. Gao, H. Dong, G.W. Zou, S.S. Han, C.L. Chow, Experimental
622 studies on fire response of glass façade systems, Int. J. Eng. Perform.-Based Fire
623 Codes 8 (2) (2006) 54-68.
624 [17] M. Debuyser, J. Sjöström, D. Lange, D. Honfi, D. Sonck, J. Belis, Behaviour of
625 monolithic and laminated glass exposed to radiant heating, Construct. Build. Mater.
626 130 (2017) 212-229
627 [18] A.A. Joshi, P.J. Pagni, Users' guide to BREAK1, the Berkeley algorithm for
628 breaking window glass in a compartment fire.
629 [19] Q. Wang, Y. Zhang, Y. Wang, J. Sun, L. He. Dynamic three-dimensional stress
630 prediction of window glass under thermal loading. Int. J. Therm. Sci.59 (2012)
631 152-160.
632 [20] Y. Wang, Q. Wang, G. Shao, H. Chen, Y. Su, J. Sun, L. He, K.M. Liew, Fracture
633 behavior of four-point fixed glass curtain wall under fire condition, Fire Saf. J.
634 67(2014) 24-34.
635 [21] P. J. Pagni, A. A. Joshi, Glass breaking in fires, in: Fire Safety Science-
636 Proceedings of the Third International Symposium, IAFSS, 1991, 791-802.
637 [22] A.A. Joshi, P.J. Pagni, Fire-Induced Thermal Fields in Window Glass.I-Theory,
638 Fire Saf. J.22 (1994) 25-43.
639 [23] P. Tofilo, M. Delichatsios, Thermally Induced Stresses in Glazing Systems, J. Fire.
640 Prot. Eng. 20 (2010) 101-116.
641 [24] H. Chen, Q. Wang, Y. Wang, H. Zhao, J. Sun, L. He. Experimental and numerical
642 study of window glass breakage with varying shaded widths under thermal loading.
643 Fire Technol. 53(2017) 43-64.
644 [25] T. J. Shields, G. W. H. Silcock, M. Flood. Performance of a single glazing
645 assembly exposed to a fire in the centre of an enclosure. Fire Mater. 26 (2002) 51-
646 75.
647 [26]E.M. Arruda, M.C. Boyce, A three-dimensional constitutive model for the large
648 stretch behavior of rubber elastic materials, J. Mech. Phys. Solids.41(1993), 389-
649 412.
650 [27] Y. Wang, Q. Wang, Y. Su, J. Sun, L. He, K.M. Liew, Fracture behavior of framing
651 coated glass curtain walls under fire conditions, Fire Saf. J.75 (2015) 45-58.
652 [28] P. J. Pagni. Thermal glass breakage. Fire Safety Science-Proceedings of the
653 Seventh International Symposium on. IAFSS, 2002:3-22.
654 [29] L. Hu, Studies on thermal physics of smoke movement in tunnel fires, in, PhD
655 Dissertation, University of Science and Technology of China, Hefei, Anhui, China,
656 2006.
657 [30] N.P. Bansal, R.H. Doremus, Handbook of Glass Properties, 1986.

[31] N.D. Pope, C.G. Bailey, Development of a Gaussian glass breakage model within a fire field model, Fire Saf. J. 42 (2007) 366-376.
[32] N. Singla, K. Jain, S. Kumar Sharma, The beta generalized Weibull distribution: properties and applications, Reliab. Eng. Syst. Saf. 102 (2012) 5-15.
[33] H.Chen, Y. Zhang, Q.Wang, Y. Wang, G.Shao, Y.Su, H. Zhao, J.Sun, L. He. Crack evolution process of window glass under radiant heating. Fire Mater. 41(2017)1-11.